International Journal of Fracture **70:** 253–266, 1995.

Notch sensitivity of fiber-reinforced ceramics

PEI GU*
Division of Engineering, Brown University, Providence, Rhode Island 02912, USA

Received 10 August 1994; accepted in revised form 24 January 1995

Abstract. Crack bridging from an elliptical hole in fiber-reinforced ceramic composites is studied. For some fiber-reinforced ceramic composites, matrix toughness is much less than the toughness gained in the bridging zone, i.e. the bridging zone runs across the entire width of a specimen at a small load. In such case, load-carrying capacity of the specimen only depends on one parameter which is the measure of notch sensitivity. Solving the crack bridging problem for various aspect ratios of the elliptical hole and various bridging law shapes, the role of crack bridging from the hole is determined. The results presented may be used to guide design in addition to providing an improved understanding of the mechanism of fiber-matrix failure.

1. Introduction

Brittle materials are reinforced by high strength fibers to produce larger tensile strength than the unreinforced brittle materials. If cracking occurs in the brittle matrix, there is a region behind the crack tip, called the bridging zone, in which fibers remain intact; these fibers in the bridging zone enhance the toughness of the composite. Research has been carried out in this area since fiber-reinforced ceramics have many applications, for example, they can be used at high temperatures. To understand this toughening mechanism, the study has been done to determine the toughness by viewing the bridging zone as a localized band which is characterized by a so-called bridging law. The bridging law is a constitutive relation between the stress and deformation of the bridging zone.

Early work using a localized band to study material failure can be traced back to the early stage of fracture mechanics when the Dugdale model [1, 2] was proposed to deal with the fracture of ductile materials. Among recent works, Marshall, Cox and Evans [3], Marshall and Cox [4], Suo, Ho and Gong [5] and Budiansky and Cui [6] have investigated the crack-bridging problem using a square-root bridging law. Reviews of recent progress in this area are given by Bao and Suo [7] and Cox and Marshall [8].

In this paper, we consider a problem as shown in Fig. 1(a), an elliptical hole in a specimen made of fiber-reinforced ceramic. Although Suo, Ho and Gong [5] have treated a circular hole problem, it is important to consider the elliptical hole problem since it is the general shape of a hole. For some fiber-reinforced ceramic composites, matrix toughness is negligible, i.e. a bridging zone initiates and extends to the boundary of the specimen at a small load. In this study, we assume the bridging zone extends over the net section of the specimen as shown in Fig. 1(a). We also assume that the size of the hole is much smaller that the size of the specimen. Then, the problem in Fig. 1(a) is reduced to an asymptotic problem shown in Fig. 1(b), where the composite is taken as infinitely large and the bridging zone is infinitely long. In the asymptotic problem, geometrical lengths are the major and minor axes of the

* Present address: Department of Applied Mechanics and Engineering Sciences, University of California at San Diego, La Jolla, CA 92093-0411, USA

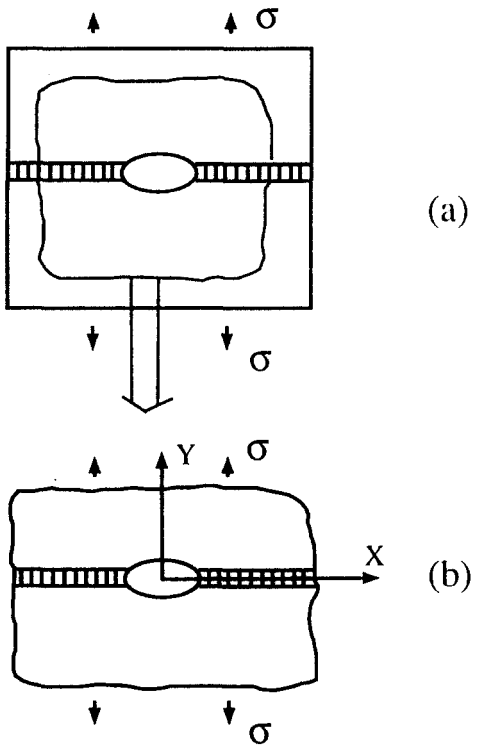

Fig. 1. Specimen geometry. (a) Finite geometry problem. (b) Asymptotic problem.

elliptical hole. Outside the bridging zone, the composite is linear elastic and isotropic; the condition of either plane strain or plane stress is applied.

We calculate load-carrying capacity of the asymptotic problem in terms of a parameter that is the measure of notch sensitivity, and we show the effects of the hole geometry and bridging law shape on load-carrying capacity. In the case of notch insensitivity, i.e. either the fiber strength is high or the hole is small, load-carrying capacity is not reduced much by presenting the hole. In the case of notch sensitivity, i.e. either the fiber strength is low or the hole is large, load-carrying capacity approaches to that obtained from an elastic hole problem without the bridging zone. Load-carrying capacity in the regime between notch sensitivity and notch insensitivity (brittle–ductile transition regime), in which many fiber-reinforced ceramics belong, is presented. Our results may be used to guide design in addition to providing an improved understanding of the mechanism of fiber-matrix failure.

2. Crack bridging

2.1 Crack bridging mechanism

A brief review of crack bridging is given here. Consider a bridging crack growing from an elliptical hole in a fiber-reinforced ceramic with still intact fibers behind the crack tip, as shown in Fig. 2. The length of the bridging zone is L, and the elliptical hole has major axis a and minor axis b. The deformation inside the bridging zone is governed by a bridging law.

$$\frac{\sigma}{\sigma_0} = \chi\left(\frac{\delta}{\delta_0}\right), \tag{1}$$

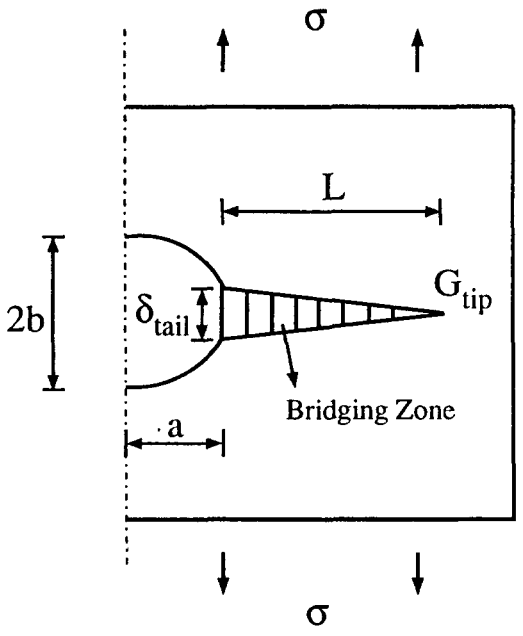

Fig. 2. Crack bridging model.

where σ and δ are the stress and stretch of the bridging zone, respectively. The bridging law sets two scales, the failure stress σ_0 and limiting stretch δ_0. It provides a means to simulate the failure of the localized zone. The failure of the bridging zone occurs when the stretch δ reaches its critical value δ_0. By considering the interfacial friction of the fiber and matrix, it has been shown that

$$\frac{\sigma}{\sigma_0} = \left(\frac{\delta}{\delta_0}\right)^{1/2}, \tag{2}$$

can be applied for fiber pull-out [3], where

$$\begin{aligned} \sigma_0 &= fS_0, \\ \delta_0 &= \frac{(1-f)RS_0^2E_m}{2\tau E_f E}. \end{aligned} \tag{3}$$

In the above two expressions, S_0 is the fiber strength, f is the fiber volume fraction, R is the fiber radius, τ is the sliding frictional stress at the fiber–matrix interface, and E_f, E_m and E are the Young's moduli of the fiber, matrix and compostie, respectively.

In a more general way, the bridging law follows the power form

$$\frac{\sigma}{\sigma_0} = \left(\frac{\delta}{\delta_0}\right)^m \quad (m \geqslant 0). \tag{4}$$

In (4), $m = 0$ corresponds to a rigid-perfectly plastic spring; $m = 1$ corresponds to a linear spring; $m = 0.5$ corresponds to (2). The three bridging law shapes are shown in Fig. 3. For the power bridging law, the bridging law shape is controlled by the exponent m.

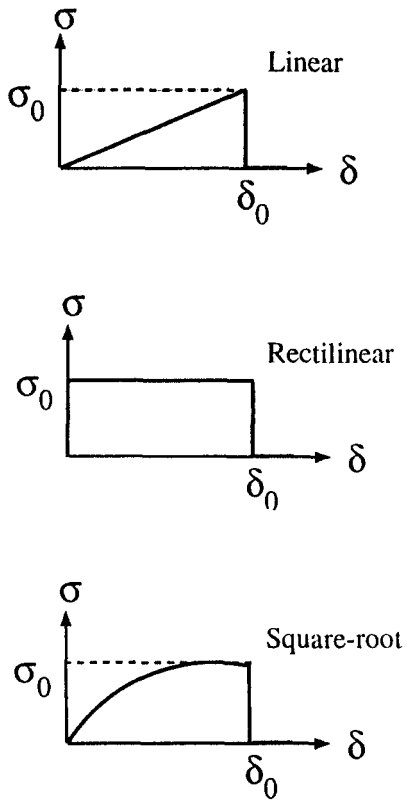

Fig. 3. Three bridging law shapes.

In general, the opening displacement at the tail of the bridging crack, δ_{tail}, and the energy release rate at the bridging crack tip, $\mathcal{G}_{\text{tip}}$, take the following forms

$$\begin{aligned} \frac{\delta_{\text{tail}}}{\delta_0} &= f\left(\frac{\sigma}{\sigma_0}, \alpha, \frac{L}{a}, \frac{b}{a}\right), \\ \frac{\mathcal{G}_{\text{tip}}}{\sigma_0 \delta_0} &= g\left(\frac{\sigma}{\sigma_0}, \alpha, \frac{L}{a}, \frac{b}{a}\right). \end{aligned} \tag{5}$$

The two functions in (5), f and g, relate to the external load, hole geometry, bridging zone length, the failure stress of the bridging zone and the parameter α. The two functions also depend on the bridging law shape. The parameter α is the hole size a normalized by a material length $E'\delta_0/\sigma_0$, i.e.

$$\alpha = \frac{a}{\delta_0 E'/\sigma_0}, \tag{6}$$

where $E' = E$ for plane stress and $E' = E/(1-\nu^2)$ for plane strain (ν is the Poisson's ratio of the composite). The material length represents fracture process zone length [9]. Failure starts as matrix cracking from the boundary of the hole. The bridging zone grows as the external load increases. The catastrophic failure is when fiber failure occurs at the boundary of the

hole, which is the tail of the bridging zone. Load-carrying capacity $\sigma_{\max}$ and the bridging zone length L can be obtained from (5) by letting $\delta_{\text{tail}} = \delta_0$ and $\mathcal{G}_{\text{tip}} = \Gamma_0$, where Γ_0 is matrix toughness. The maximum load is given in the form

$$\frac{\sigma_{\max}}{\sigma_0} = \mathcal{P}\left(\alpha, \frac{L}{a}, \frac{b}{a}\right). \tag{7}$$

The function $\mathcal{P}$ also depends on the bridging law shape.

The parameter α is the measure of notch sensitivity. It represents the competition between elastic stress concentration caused by the hole and inelastic stress relaxation caused by the crack bridging, since it is the hole size measured in units of the fracture process zone length. When $\alpha = 0$, there is no stress concentration (a crack parallel to the loading direction), or the fracture process zone length is infinite; so, load-carrying capacity is not reduced in this case, i.e. $\sigma_{\max} = \sigma_0$. When α is infinitely large, the hole size a is infinitely large, or the fracture process zone length is zero; so, there is no bridging effect, i.e. $\sigma_{\max} = \eta\sigma_0$, where η is the inverse of the stress concentration factor of the hole. For example, the stress concentration factor of a circular hole is 3, so load-carrying capacity is one third of σ_0 for a circular hole with $\alpha = \infty$. If α is small, a specimen is said to be notch insensitive; if α is large, it is said to be notch sensitive. There is a regime between notch insensitivity and notch sensitivity, where load-carrying capacity is between $\eta\sigma_0$ and σ_0; it is the regime of brittle–ductile transition. The reduction of load-carrying capacity in this regime only depends on the parameter α for a given aspect ratio of the elliptical hole. Both the hole size α and the material length $\delta_0 E'/\sigma_0$ are important to control notch sensitivity. Given a hole size, a large $\delta_0 E'/\sigma_0$ reduces notch sensitivity and a small $\delta_0 E'/\sigma_0$ increases notch sensitivity. For fiber pull-out, the material length is in the order of 1 mm [7]. Given a material length, a large hole increases notch sensitivity and a small hole reduces notch sensitivity. From the design point of view, we would like α to be as small as possible so a component can sustain high external load. This can be achieved by either avoiding large holes or selecting composites with large values of the material length.

The fiber failure at the tail of the bridging zone can occur at a finite bridging zone length or at an infinite bridging zone length. At the early stage of loading, the bridging zone length increases as the external load increases. Fiber failure occurs if the stretch δ at the tail of the bridging zone reaches its limiting value δ_0, and load-carrying capacity is the external load corresponding to the fiber failure. If the fiber failure does not occur, the external load increases to reach a peak value and then decreases to approach the steady-state matrix-cracking stress at the bridging zone length $L = \infty$ [6, 10]. The external load can still increase at $L = \infty$ if the fiber failure still does not occur at this time, and this is the problem shown in Fig. 1, which we shall study in this paper. This is the case that matrix toughness is very small so the bridging zone runs across the entire width of the specimen at a small load. In this case, (7) takes the form

$$\frac{\sigma_{\max}}{\sigma_0} = \mathcal{F}\left(\alpha, \frac{b}{a}\right), \tag{8}$$

where $\mathcal{F}$ also depends on the bridging law shape.

2.2. PROBLEM FORMULATION

The mathematical problem shown in Fig. 1(b) is considered. A bridging zone emanates from $x = \pm a$ and coincides with the x axis. Far from the hole, the hole's effect vanishes so the opening displacement of the bridging crack approaches to

$$\frac{\delta_{\pm\infty}}{\delta_0} = \chi^{-1}\left(\frac{\sigma}{\sigma_0}\right), \tag{9}$$

as $x \to \pm\infty, y = 0$. At an arbitrary point on the x axis, $x > a, y = 0$, we have the following expression for the opening displacement of the bridging crack

$$\frac{\delta(x)}{\delta_0} = \chi^{-1}\left(\frac{\sigma}{\sigma_0}\right) + \int_x^{+\infty} b(\xi)\,\mathrm{d}\xi, \tag{10}$$

where

$$b(\xi) = -\frac{\partial\delta(\xi)}{\delta\xi}. \tag{11}$$

In order to have a finite opening displacement, $b(\xi)$ decays in the order

$$b(\xi) = O\left(\frac{1}{\xi^2}\right), \tag{12}$$

as $\xi \to \pm\infty$. The condition (12) guarantees that the integral in (10) is well defined. The deformation of the bridging zone is simulated by an array of dislocations, and the dislocation density is given by (11). The stress in the bridging zone at the position, $x > 1, y = 0$, is equal to the stress due to the external load plus that due to the dislocation array. This relation leads to an integral equation

$$\chi\left[\chi^{-1}\left(\frac{\sigma}{\sigma_0}\right) + \int_x^{\pm\infty} b(\xi)\,\mathrm{d}\xi\right] = \frac{\sigma}{\sigma_0}F(x) + \frac{1}{\alpha}\int_1^{+\infty}[H(x,\xi) - H(x,-\xi)]b(\xi)\,\mathrm{d}\xi \tag{13}$$

for $x > 1$. In deriving this equation, $b(\xi)$ is normalized by δ_0/a; x and ξ are normalized by a. These normalizations will be used in following derivations. The function $F(x)$ is σ_{yy} at the position, $x > 1, y = 0$, in the solution to an elliptic hole in a plate subjected to a unit remote load $\sigma = 1$, which can be found in [11]; and $H(x,\xi)$ is σ_{yy} at the position, $x > 1, y = 0$, due to a single unit dislocation at $\xi > 1$ (or $\xi < -1$), $y = 0$, in a plate with an elliptic hole. To obtain the solution to the dislocation problem, the two complex potentials of linear elasticity can be written as

$$\begin{aligned}\phi(z) &= \phi_0(z) - \phi_*(z),\\ \psi(z) &= \psi_0(z) - \psi_*(z).\end{aligned} \tag{14}$$

In (14), $\phi_0(z)$ and $\psi_0(z)$ are the solution to a single dislocation in an infinite homogeneous plate without the hole; the second terms, $\phi_*(z)$ and $\psi_*(z)$, are used to adjust the first two

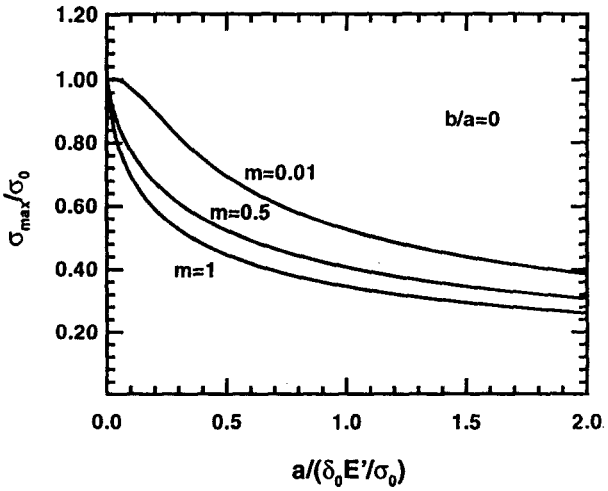

Fig. 4. Load-carrying capacity versus notch sensitivity for $b/a = 0$.

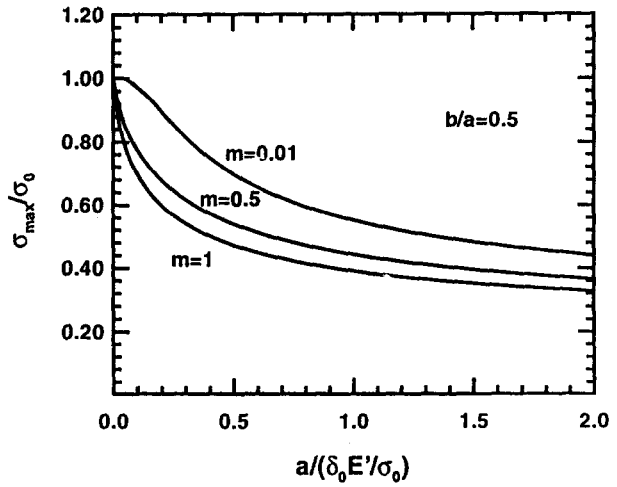

Fig. 5. Load-carrying capacity versus notch sensitivity for $b/a = 0.5$.

potentials so $\phi(z)$ and $\psi(z)$ satisfy the traction-free condition on the boundary of the elliptical hole. Expressions for $\phi_*(z)$ and $\psi_*(z)$, which can be found in [12], are given in Appendix A. Expression for $H(x, \xi)$ is given in Appendix B. The term $H(x, -\xi)$ is the contribution from the other branch of the bridging zone, $x < -1$, in Fig. 1(b).

In order to determine load-carrying capacity, an additional equation for the fiber failure is required. The maximum load $\sigma_{\max}$ is attained when the opening displacement at the tail of

the bridging crack, δ_{tail}, reaches its maximum value, δ_0. The opening displacement δ_{tail} can be written in terms of the external load σ and the dislocation density $b(\xi)$ as

$$\frac{\delta_{\text{tail}}}{\delta_0} = \chi^{-1}\left(\frac{\sigma}{\sigma_0}\right) + \int_1^{\infty} b(\xi)\,\mathrm{d}\xi. \tag{15}$$

The maximum load $\sigma_{\max}$ together with the dislocation density are solved from integral equations (13) and (15) by letting $\delta_{\text{tail}} = \delta_0$ in (15). The maximum load is given in the form

$$\frac{\sigma_{\max}}{\sigma_0} = \mathcal{F}^*(\alpha), \tag{16}$$

for the given aspect ratio b/a and bridging law shape. Equation (16) reconfirms that α is the parameter measuring notch sensitivity.

The solution for $\sigma_{\max}$ can be determined analytically in the following special cases:

(a) If $\alpha = \infty$, we have from (13) that

$$\chi^{-1}\left(\frac{\sigma_{\max}}{\sigma_0}\right) + \int_1^{+\infty} b(\xi)\,\mathrm{d}\xi = \chi^{-1}\left[\frac{\sigma_{\max}}{\sigma_0}F(1)\right]. \tag{17}$$

Substituting (17) into (15) yields

$$1 = \chi^{-1}\left[\frac{\sigma_{\max}}{\sigma_0}F(1)\right]. \tag{18}$$

Noting that $\chi(1) = 1$, (18) can be rearranged as

$$\frac{\sigma_{\max}}{\sigma_0} = \eta = \frac{1}{F(1)}, \tag{19}$$

where $F(1)$ is the stress concentration factor of the elliptical hole. This agrees with the analysis in Section 2.1.

(b) If $\alpha = 0$, we have from (13) that

$$b(\xi) = 0. \tag{20}$$

Then, (15) gives

$$\frac{\sigma_{\max}}{\sigma_0} = 1. \tag{21}$$

This also agrees with the analysis in Section 2.1.

(c) If $b/a = \infty$, this is equivalent to the case $\alpha = 0 (a = 0)$. So, the maximum load is still given by (21).

In the above three cases, the maximum load is independent of the bridging law shape.

3. Numerical solution

For general values of α, (13) and (15) are solved numerically to determine $\sigma_{\max}$. We obtain algebraic equations using the Gauss–Chebyshev quadrature rule developed by Erdogan and Gupta [13]. The Gauss–Chebyshev quadrature rule was modified by Lo [14] to solve the

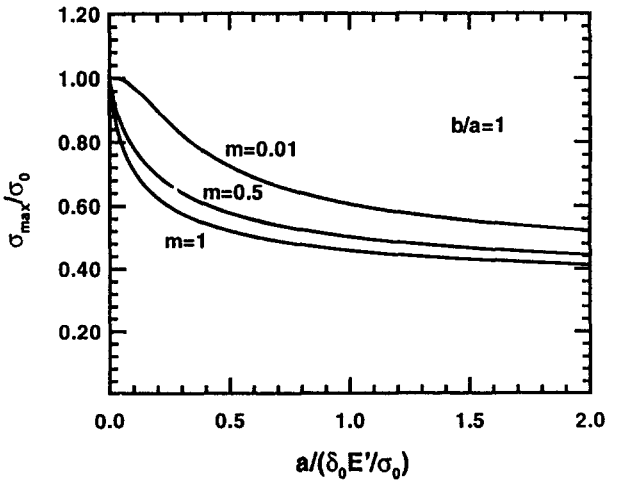

Fig. 6. Load-carrying capacity versus notch sensitivity for $b/a = 1$.

crack kinking problem. Lo's treatment of no singularity at the original crack tip is employed here since we do not have a singularity at the boundary of the hole, $\xi = 1$. Also, there is no singularity at $\xi = +\infty$ according to (12). These requirements can be satisfied by writing $b(\xi)$ in the following form

$$b(t) = \frac{(1-t)^{5/2} f(t)}{\sqrt{1-t^2}}, \tag{22}$$

using a transformation

$$\xi = \frac{2}{1-t}, \tag{23}$$

where $-1 < t < 1$ and $f(t)$ is a regular function (continuous, without singularity). In (22), $b(t) \to \infty$ if $t \to -1(\xi \to 1)$. Using Lo's treatment, we enforce $f(-1) = 0$ to remove the singularity. Note that (22) does not have a singularity at $t = 1(\xi = +\infty)$. The resulting nonlinear algebraic equations from the Gauss–Chebyshev quadrature rule are solved by the Newton–Raphson method. Details about the numerical procedure is given in Appendix B. The convergence of the numerical method is very satisfactory. If 90 quadrature points are used, the error is less than 0.2 percent. In addition, we check the accuracy of the method by letting α and b/a be equal to, or approach, the particular cases whose solutions are analytically given in the last section. Comparison of solutions obtained from the two methods gives us more confidence about our numerical scheme.

An appropriate bridging law to represent the constitutive relation of the bridging zone is very important to understanding the fracture mechanism of fiber-reinforced ceramics. Assuming both the fiber and matrix are linear elastic and the interfacial friction stress between the fiber and matrix is a constant over the region of slipping, it has been shown that the exponent m in (4) is equal to 0.5 for fiber pull-out [3, 15]. On the other hand, other bridging law shapes, linear and rectilinear, can also be used to study crack bridging and other problems. The linear

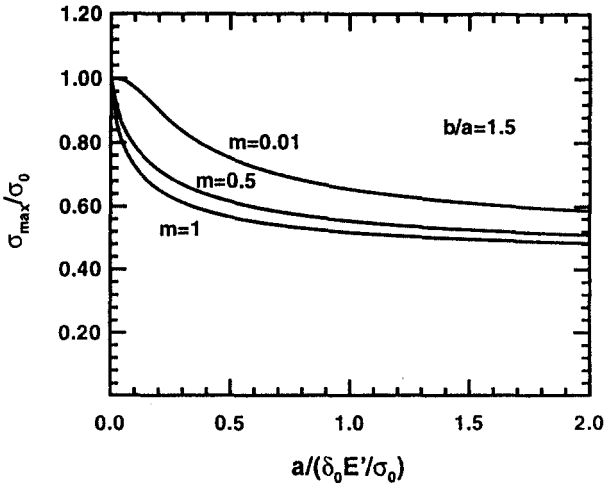

Fig. 7. Load-carrying capacity versus notch sensitivity for $b/a = 1.5$.

bridging law is used by Rose [16] and Budiansky, Amazigo and Evans [17]; the rectilinear bridging law is used in the Dugdale model and other works. At this time, we would like to examine the effect of the bridging law shape on load-carrying capacity. To do this, plots of $\sigma_{\max}/\sigma_0$ versus α for $m = 0.01, 0.5$ and 1 are shown in Figs, 4, 5, 6 and 7 for the cases of $b/a = 0, 0.5, 1$ and 1.5, respectively. It can be seen that load-carrying capacity decreases rapidly with increasing α for small α, and the decrease becomes slow for large α. This is particularly true for $m = 0.5$ and 1. The case for $m = 0.01$ is somewhat different: at very small α the decrease of load-carrying capacity is slow, then the decrease becomes fast as α increases and slow again at large α. In each of these figures, load-carrying capacity increases as m decreases. This is because the smaller m means more fracture energy in the bridging zone. The difference in these plots between $m = 0.5$ and 1 is less than the difference between $m = 0.5$ and 0.01.

We examine the effect of the hole geometry on load-carrying capacity. In practice, an arbitrary hole shape may be found in a fiber-reinforced ceramic composite. The hole shape depends on many factors which are mainly related to manufacturing process and the application of the composite. An ellipse is enough for understanding the effect of a hole from the mechanics point of view, since it results in stress singularity and stress concentrations which the hole can have as b/a varies from 0 to ∞. For comparison, the maximum stress $\sigma_{\max}$ for several b/a's are shown in Figs. 8, 9 and 10 for the cases of $m = 0.01, 0.5$ and 1, respectively. Load-carrying capacity is reduced as b/a decreases from ∞ to 0, and the lowest $\sigma_{\max}$ is attained when $b/a = 0$ (crack). This is because the smaller aspect ratio results in the larger stress concentration near the tail of the bridging zone, and the crack has the largest stress concentration, i.e. stress singularity. The geometry effect becomes significant for large α. This is because load-carrying capacity is inversely proportional to the stress concentration factor of the elliptical hole as α approaches infinity, where different b/a's have different stress concentration factors. The hole geometry has little influence on $\sigma_{\max}$ for small α. It can be seen in Fig. 9 that, if $\alpha \leqslant 0.2$, elliptical holes with aspect ratios b/a between 0 and 1 have almost the same $\sigma_{\max}$. This means that there is a value of α, namely α^*, such that for a small hole or

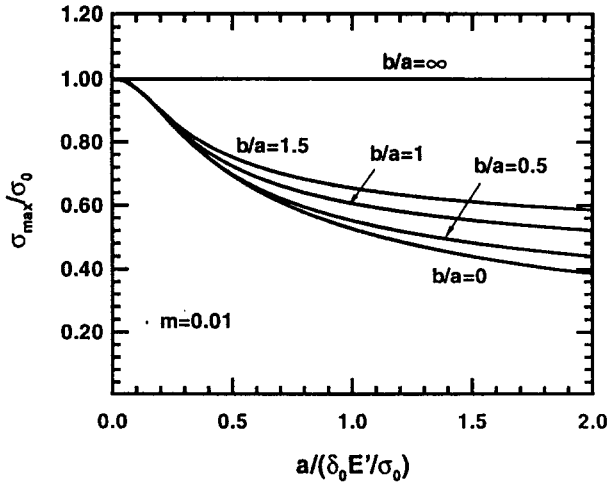

Fig. 8. Geometry effect on load-carrying capacity for $m = 0.01$.

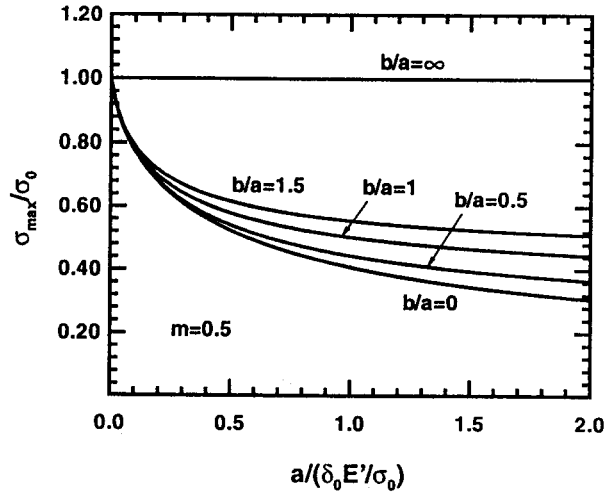

Fig. 9. Geometry effect on load-carrying capacity for $m = 0.5$.

a large material length which gives $\alpha \leqslant \alpha^*$, it is not necessary to distinguish whether the hole shape is ellipse, circle or crack as far as load-carrying capacity is concerned. Note that for a homogeneous ceramic plate, a circular hole, even if it is very small, reduces load-carrying capacity to one third of the strength of the material; an elliptical hole with $a/b = 2$, even if it is very small, reduces load-carrying capacity to one fifth of the strength of the material (the stress concentration factor for the elliptical hole is 5). In other words, a fiber-reinforced ceramic has the hole size effect while a homogeneous ceramic does not. This is one of the advantages of using composites! We also find from these figures that different m gives different α^*, for example, α^* is about 0.3 in Fig. 8, the case for $m = 0.01$.

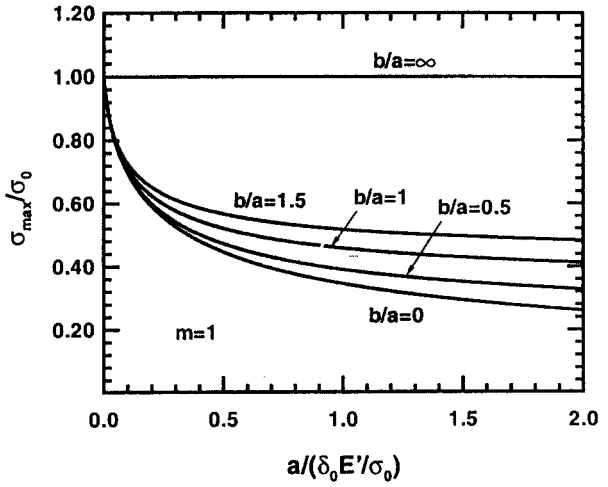

Fig. 10. Geometry effect on load-carrying capacity for $m = 1$.

We compare our solution in the case of a crack ($b/a = 0$) and rectilinear bridging law with the solution to the Dugdale model. In the Dugdale model, the plastic-zone length together with load-carrying capacity are determined by letting the stress intensity factor at the tip of the plastic zone be equal to zero and specifying a critical opening displacement at the tail of the plastic zone, δ_0. This gives an analytic solution

$$\frac{\sigma_{\max}}{\sigma_0} = \frac{2}{\pi} \sec^{-1} e^{\pi/(8\alpha)}. \tag{24}$$

In our integral equations, (13) and (15), the rectilinear bridging law can be approached by letting the exponent m be sufficiently close to 0. It is interesting that the difference between the two solutions in the interval $0 \leqslant \alpha \leqslant 2$ is so small that we can not see it in a plot. In other words, in this interval, the solution to the Dugdale model may be viewed as an upper bound for load-carrying capacity in our integral equation solution for $m > 0$.

4. Concluding remarks

Crack bridging near an elliptical hole is solved and its solution is presented in terms of the notch-sensitivity parameter $a/(\delta_0 E'/\sigma_0)$. The effects of the hole geometry and bridging law shape on load-carrying capacity of a specimen are determined. It is found that the hole geometry has a strong effect on load-carrying capacity for large $a/(\delta_0 E'/\sigma_0)$, and the geometry effect is negligible for small $a/(\delta_0 E'/\sigma_0)$. The bridging law shape also has an effect on load-carrying capacity, i.e. the smaller exponent m in the power bridging law gives the higher load-carrying capacity. Our solution provides a lower bound when matrix toughness is considered, since we neglect matrix toughness and assume the bridging zone runs far away from the boundary of the hole in the present formulation. Nevertheless, this gives a good prediction for those fiber-reinforced ceramics with small values of matrix toughness.

We also take the composite as an isotropic body in our calculation. The work to consider the orthotropy of the composite is done by Cui [18] for the case $m = 0.5$. For numerous

values of the moduli of the fiber and matrix, the values of the two parameters measuring the orthotropy are not far from those in the isotropic case, as noted in [18]. So, we do not expect the orthotropy of these composites to have a strong effect on load-carrying capacity.

Appendix A

We write the two complex potentials of linear elasticity for an edge dislocation at z_0 in an infinite plate with an elliptical hole in the following form

$$\begin{aligned} \phi(z) &= \phi_0(z) - \phi_*(z), \\ \psi(z) &= \psi_0(z) - \psi_*(z), \end{aligned} \tag{A.1}$$

where $\phi_0(z)$ and $\psi_0(z)$ denote the solution to the dislocation in an infinite, homogeneous plate without the hole. The solutions for $\phi_*(z)$ and $\psi_*(z)$ are obtained as

$$\begin{aligned} \phi_*(\zeta) &= -\gamma \log\left\{\frac{\zeta - m/\zeta_0}{\zeta}\right\} - \gamma \log\left\{\frac{\zeta - 1/\bar{\zeta}_0}{\zeta}\right\} \\ &\quad + \frac{\bar{\gamma}}{m}\frac{(1/\bar{\zeta}_0 - m/\zeta_0)(1/\bar{\zeta}_0 - \zeta_0)}{(1/\bar{\zeta}_0 - \bar{\zeta}_0/m)(1/\bar{\zeta}_0 - \zeta)}, \\ \psi_*(\zeta) &= -\bar{\gamma} \log\left\{\frac{\zeta - 1/\bar{\zeta}_0}{\zeta}\right\} - \bar{\gamma} \log\left\{\frac{\zeta - m/\zeta_0}{\zeta}\right\} \\ &\quad + \gamma m \frac{(m/\zeta_0 - 1/\bar{\zeta}_0)(m/\zeta_0 - \bar{\zeta}_0/m)}{(m/\zeta_0 - \zeta_0)(m/\zeta_0 - \zeta)} - \zeta \frac{1 + m\zeta^2}{\zeta^2 - m}\phi_*'(\zeta), \end{aligned} \tag{A.2}$$

where

$$\gamma = \frac{\mu \mathbf{b}}{i\pi(\kappa + 1)}, \tag{A.3}$$

and

$$\begin{aligned} m &= \frac{a - b}{a + b}, \qquad R = \frac{a + b}{2}, \\ z &= R\left(\zeta + \frac{m}{\zeta}\right), \qquad z_0 = R\left(\zeta_0 + \frac{m}{\zeta_0}\right). \end{aligned} \tag{A.4}$$

In these expressions, $\mathbf{b}$ is the Burgers vector; μ is the shear modulus; $\kappa = 3 - 4\nu$ for plane strain, and $\kappa = (3 - \nu)/(1 + \nu)$ for plane stress. The mapping is chosen such that the region outside the elliptical hole in the z plane is mapped onto the region outside the unit circle in the ζ plane.

Appendix B

The function $H(x, \xi)$ in (13) is σ_{yy} at $x (x \geqslant 1)$ due to a single unit dislocation at $\xi (\xi \geqslant 1)$, calculated from the two potentials $\phi(z)$ and $\psi(z)$ in Appendix A. Using the following variable changes

$$x = \frac{2}{1 - u}, \qquad \xi = \frac{2}{1 - t}, \tag{A.5}$$

the integral equation (13) can be written as

$$\int_{-1}^{1} \frac{b(t)}{u-t}\,\mathrm{d}t - \int_{-1}^{1} \frac{b(t)}{1-t}\,\mathrm{d}t - \int_{-1}^{1} \frac{(1-u)b(t)}{(2-t-u)(1-t)}\,\mathrm{d}t$$

$$+ \int_{-1}^{1} \left[G\left(\frac{2}{1-u}, \frac{2}{1-t}\right) - G\left(\frac{2}{1-u}, -\frac{2}{1-t}\right) \right] \frac{b(t)}{(1-t)^2}\,\mathrm{d}t$$

$$+ 4\pi\alpha \frac{\sigma}{\sigma_0} F\left(\frac{2}{1-u}\right) - 4\pi\alpha \left[\left(\frac{\sigma}{\sigma_0}\right)^{1/m} + 2\int_{u}^{1} \frac{b(t)}{(1-t)^2}\,\mathrm{d}t \right]^{m},$$

$$= 0, \tag{A.6}$$

where $G(x, \xi)$ is σ_{yy} calculated from the two potentials $\phi_*(z)$ and $\psi_*(z)$ in Appendix A.

We solve load-carrying capacity $\sigma_{\max}$ from (A.6) and (15). As we discussed in the beginning of Section 3, $b(t)$ may be written in the form

$$b(t) = \frac{(1-t)^{5/2} f(t)}{\sqrt{1-t^2}}, \tag{A.7}$$

where $f(t)$ is a regular function to be determined. The Gauss–Chebyshev quadrature rule [13] is used to obtain algebraic equations from (A.6) and (15). There are $N+1$ unknowns if we use N quadrature points: σ and $f_i (i = 1, 2, \ldots, N; f_i$ denotes $f(t)$ at the quadrature point). On the other hand, there are $N+1$ algebraic equations from (A.6), (15) and the condition that there is no singularity at $t = -1$ [14]. Thus, the system is solvable and it is solved by the Newton–Raphson method.

Acknowledgements. This work is supported by the Office of Naval Research through Grant N00014-90-J-1380. Discussions with Professor C.F. Shih, Z. Suo and Dr. Y.L. Cui are gratefully acknowledged.

References

1. D.S. Dugdale, *Journal of the Mechanics and Physics of Solids* 8 (1960) 100–104.
2. G.I. Barenblatt, *Advances in Applied Mechanics* 7 (1962) 55–129.
3. D.B. Marshall, B.N. Cox and A.G. Evans, *Acta Metallurgica* 33 (1985) 2013–2021.
4. D.B. Marshall and B.N. Cox, *Acta Metallurgica* 35 (1987) 2607–2619.
5. Z. Suo, S. Ho and X. Gong, *ASME Journal of Engineering Materials and Technology* 115 (1992) 319–326.
6. B. Budiansky and Y.L. Cui, *Journal of the Mechanics and Physics of Solids* 42 (1994) 1–19.
7. G. Bao and Z. Suo, *Applied Mechanics Reviews* 45 (1992) 355–366.
8. B.N. Cox and D.B. Marshall, *Acta Metallurgica* 42 (1994) 341–363.
9. B.A. Bilby, A.H. Cottrell and K.H. Swinden, *Proceedings of the Royal Society of London* A272 (1963) 304–314.
10. J. Aveston, G.A. Cooper and A. Kelly, in *The Properties of Fiber Composites*, Proceedings of National Physical Laboratory, IPC Science and Technology (1971).
11. N.I. Muskhelishvili, *Some Basic Problems in the Mathematical Theory of Elasticity*, Noordhoff (1953).
12. V. Vitek, *Journal of the Mechanics and Physics of Solids* 24 (1975) 67–76.
13. F. Erdogan and G.D. Gupta, *Quarterly of Applied Mathematics* 29 (1972) 525–534.
14. K.K. Lo, *ASME Journal of Applied Mechanics* 45 (1978) 797–802.
15. J.W. Hutchinson and H.M. Jensen, *Mechanics of Materials* 9 (1990) 139–163.
16. L.R.F. Rose, *Journal of the Mechanics and Physics of Solids* 35 (1987) 383–405.
17. B. Budiansky, J.C. Amazigo and A.G. Evans, *Journal of the Mechanics and Physics of Solids* 36 (1988) 167–187.
18. Y.L. Cui, *Mechanics of Materials*, to appear.